Spin-State Crossover and Hyperfine Interactions of Ferric Iron in $MgSiO_3$ Perovskite

Han Hsu,[1] Peter Blaha,[2] Matteo Cococcioni,[1] and Renata M. Wentzcovitch[1]

[1]*Department of Chemical Engineering and Materials Science, University of Minnesota, Minneapolis, Minnesota, USA*
[2]*Institute of Materials Chemistry, Vienna University of Technology, A-1060 Vienna, Getreidemarkt 9/165-TC, Austria*

(Received 10 December 2010; published 14 March 2011)

Using density functional theory plus Hubbard U calculations, we show that the ground state of (Mg, Fe)(Si, Fe)O_3 perovskite, the major mineral phase in Earth's lower mantle, has high-spin ferric iron ($S = 5/2$) at both dodecahedral (A) and octahedral (B) sites. With increasing pressure, the B-site iron undergoes a spin-state crossover to the low-spin state ($S = 1/2$) between 40 and 70 GPa, while the A-site iron remains in the high-spin state. This B-site spin-state crossover is accompanied by a noticeable volume reduction and an increase in quadrupole splitting, consistent with recent x-ray diffraction and Mössbauer spectroscopy measurements. The anomalous volume reduction leads to a significant softening in bulk modulus during the crossover, suggesting a possible source of seismic-velocity anomalies in the lower mantle.

DOI: 10.1103/PhysRevLett.106.118501 PACS numbers: 91.60.Pn, 76.80.+y, 91.60.Fe, 91.60.Gf

The total electron spin (S) of a transition-metal ion in a crystalline solid can change with many factors, such as pressure, strain, or temperature, to name a few. This phenomenon, known as spin-state crossover, is of great importance in spintronics, as it allows artificial control of magnetic properties of materials, including coordination complexes with potential for molecular switches [1]. Not as widely known, spin-state crossover also plays a crucial role in geophysics. A well-studied example is ferropericlase, (Mg,Fe)O, the second most abundant mineral (~ 20 vol %) in the largest single region (~ 55 vol %) of Earth's interior—the lower mantle. With increasing pressure, ferrous iron (Fe^{2+}) in this mineral undergoes a crossover from high-spin (HS) state, $S = 2$, to low-spin (LS) state, $S = 0$, in the pressure range of 40–55 GPa [2–6]. The intermediate-spin (IS) state, $S = 1$, is not observed in this mineral. The HS-LS crossover in ferropericlase directly affects the structural, elastic, optical, and conducting properties of this mineral [6–11] and thus affects mantle properties [10,12,13].

In contrast, the spin-state crossover in iron-bearing magnesium silicate ($MgSiO_3$) perovskite (Pv), the most abundant mineral (~ 75 vol %) in the lower mantle, has been a source of controversy for two main reasons. One reason is the coexisting ferrous and ferric iron (Fe^{3+}) in this mineral with an imprecisely estimated population ratio, the other is the lack of definitive tools to directly probe iron spin state at high pressures. Two techniques, x-ray emission spectroscopy (XES) and Mössbauer spectroscopy, have been widely used, but their interpretation can be ambiguous. The very similar XES spectra [14,15] and Mössbauer spectra [16–19] have been interpreted in terms of HS-IS and HS-LS crossover in (Mg, Fe)SiO_3 Pv. Plenty of calculations on (Mg, Fe)SiO_3 Pv have been conducted [20–25], but consistency with experiments was not achieved until very recently [26,27]. Now the spin state in (Mg, Fe)SiO_3 Pv is better understood: the observed increase of iron nuclear quadrupole splitting (QS) in Mössbauer spectra results from neither HS-IS nor HS-LS crossover, but from the change in the $3d$ orbital occupancy of the HS iron [27]. As to ferric iron in Pv, possibly more abundant than ferrous iron ($Fe^{3+}/\sum Fe$ might be as high as 2/3) [28,29], its spin-state crossover has remained unclear, as described below.

Previous experiments investigating the iron spin state in aluminum-free $MgSiO_3$ Pv were focused mostly on ferrous iron [16,18]. Nevertheless, it was still observed that the low concentration of ferric iron in the sample exhibited an increase in QS with pressure, which suggests a crossover from HS ($S = 5/2$) to LS ($S = 1/2$) state in the pressure range of 30–70 GPa. In contrast, in Al-bearing samples, where ferric iron occupies the dodecahedral (A) site, the QS remains unchanged up to 100 GPa, which suggests the A-site iron remains in the HS state [17]. These results indicate that the ferric iron at the octahedral (B) site undergoes a spin-state crossover. A recent experiment using $(Mg_{1-x}Fe_x)(Si_{1-x}Fe_x)O_3$ Pv ($x = 0.1$) samples supports such a mechanism: about half of the HS iron changes to LS state in the 45–60 GPa range while the other half remain in the HS state all the way to 150 GPa [30]. So far, the computational studies on $(Mg_{1-x}Fe_x)(Si_{1-x}Fe_x)O_3$ Pv have found a ground state with HS iron at the A site and LS iron at the B site (A HS, B LS) and an A-site HS-LS crossover that leads both A- and B-site iron to a final LS state (A LS, B LS) at high pressures [21,22]. These predictions are inconsistent with experiments in two ways: (1) the predicted transition pressure is too high and (2) the predicted HS iron concentration is too low.

To compare with recent experiments [30], we stabilize $(Mg_{1-x}Fe_x)(Si_{1-x}Fe_x)O_3$ Pv with $x = 0.125$ in all possible spin states using a 40-atom supercell shown in Fig. 1. We also calculate the iron nuclear electric field gradient

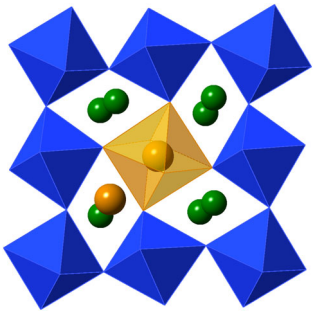

FIG. 1 (color online). Atomic structure of $(Mg_{0.875}Fe_{0.125})(Si_{0.875}Fe_{0.125})O_3$ Pv, configured with the shortest iron-iron distance, viewing along the [001] direction. Large (orange) and small (green) spheres represent Fe and Mg sites, respectively. Si-O and Fe-O octahedra are shown in opaque [dark (blue)] and translucent [light (orange)] colors.

(EFG) associated with each state, as the nuclear hyperfine interaction has proven to be a unique fingerprint to identify the spin states of transition-metal ions [27,31]. The atomic structures were fully optimized with damped variable cell shape molecular dynamics [32] implemented in the QUANTUM ESPRESSO code [33], where the plane-wave pseudopotential method is adopted [34]. These states were also independently confirmed via the augmented plane-wave plus local orbitals (APW + lo) method [35] implemented in the WIEN2K code [36], with which the EFGs were calculated. The EFGs were converted to QSs with ^{57}Fe nuclear quadrupole moment $Q = 0.16$ [37] and 0.18 b for the possible uncertainty. To treat $(Mg_{1-x}Fe_x)(Si_{1-x}Fe_x)O_3$ Pv, the density functional theory plus Hubbard U (DFT + U) method is necessary, as standard DFT exchange-correlation functionals, the local density approximation (LDA) and generalized gradient approximation (GGA), sometimes lead to unwanted metallic states (especially at high pressures), in which the iron spin states are not well defined. Since the Hubbard U of A- and B-site iron in each spin state is unknown, we have to stabilize the desired spin state with a trial U and then extract the self-consistent U, referred to as U_{sc}, using the linear response approach [38] in a recently developed iterative procedure. This procedure is equivalent to, but more efficient than, the one published earlier [39], and has been successfully implemented [40]. More details are described in the supplemental material [41].

Within DFT + U, several combinations of iron spin states can be stabilized. The A-site ferric iron can be stabilized in HS, IS, and LS states. The B-site ferric iron can be stabilized not only in LS state, but also in HS state that was not found in previous calculations [21,22]. The spin moments of the A- and B-site iron can be either parallel or antiparallel. The U_{sc} of ferric iron in Pv, listed in Table I, mainly depends on the iron spin state, slightly depends on the occupied site, and barely depends on pressure and alignment of spin moments.

The relative enthalpy (ΔH) of each stabilized state is shown in Fig. 2, where the previously perceived ground state (A HS, B LS) [21,22] is used as a reference. Remarkably, the actual ground state of (Mg, Fe)(Si, Fe)O_3 Pv has HS iron on both sites (A HS, B HS), regardless of the choice of exchange-correlation functional (LDA or GGA) and Hubbard U (U_{sc} or 4 eV). These choices do not affect the spin-state crossover either: an HS-LS crossover only occurs in the B-site iron, while the A-site iron remains HS. As expected, the predicted transition pressure (P_T) depends on the exchange-correlation functional and Hubbard U: with LDA + U_{sc}, $P_T = 41$ GPa; with GGA + U_{sc}, $P_T = 70$ GPa; with GGA + U ($U = 4$ eV), $P_T = 29$ GPa. (Coordination complexes also show similar dependence [42,43].) Notably, the alignment of iron spins (parallel or antiparallel) barely affects P_T, as shown in Fig. 2(c). The P_T predicted by LDA + U_{sc} and GGA + U_{sc} best agree with the P_T observed in Mössbauer spectra: 50–60 GPa [30]. The LDA + U_{sc} electronic density of states (DOS) of the two relevant states (A HS, B HS and A HS, B LS) can be found in the supplemental material [41].

The calculated QSs of ferric iron (A and B site) and ferrous iron (A site) [27] in various spin states, along with the measured QSs [16,18,30], are shown in Fig. 3. Clearly, our calculations on ferrous and ferric iron in Pv are consistent with Mössbauer spectra. The HS-LS crossover in the B-site ferric iron also helps to explain the decrease in XES satellite peak ($K\beta'$) intensity [14,15]. Interestingly, the QS of ferrous and ferric iron exhibit exactly the opposite trends with respect to the spin moment. This can be understood via their orbital occupancies. The LS ferrous iron, although occupying the A site, is effectively located near the center of a Fe-O octahedron, as it is vertically displaced from the mirror plane [24]. Its six $3d$ electrons doubly occupy the three orbitals with t_{2g} character and form a charge density with cubiclike shape [24], which barely contributes to the EFG and leads to a very small QS. The HS ferric iron also has a small EFG (and thus QS), irrespective of A or B site. This is because its five $3d$ electrons (all spin-up) occupy all $3d$ orbitals, forming an almost spherically shaped electron charge distribution that leads to a small EFG (and thus QS). Similarly, the spin-up electrons in HS ferrous and LS ferric iron barely contribute to EFG, as their charge distributions are nearly spherical and cubic, respectively. It is their spin-down electrons that contribute to the EFGs and lead to larger QSs. This is why the spin moments of ferrous and ferric iron appear to affect the QSs in an opposite manner.

TABLE I. U_{sc}, the self-consistent Hubbard U (in eV), of ferric iron on the A and B site in each spin state.

	A site	B site
HS ($S = 5/2$)	3.7	3.3
IS ($S = 3/2$)	4.6	-
LS ($S = 1/2$)	5.2	4.9

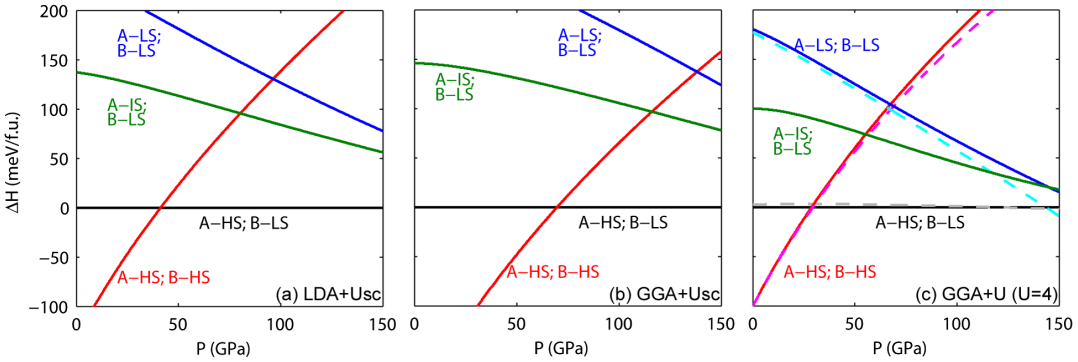

FIG. 2 (color online). Relative enthalpies of $(Mg_{0.875}Fe_{0.125})(Si_{0.875}Fe_{0.125})O_3$ Pv in different spin states obtained using different functionals and Hubbard U. The reference state has HS iron in the A site and LS iron in the B site (A HS, B LS). Predicted transition pressures by LDA + U_{sc} (a), GGA + U_{sc} (b), and GGA + U with $U = 4$ eV (c) are 41, 70, and 29 GPa, respectively. Dashed lines in (c) correspond to antiparallel spins at A and B sites.

The LDA + U_{sc} compression curves and bulk modulus ($K \equiv -VdP/dV$) of $(Mg_{1-x}Fe_x)(Si_{1-x}Fe_x)O_3$ Pv ($x = 0.125$) along with the experimental data ($x = 0.1$) [30] are shown in Fig. 4. At low pressures (< 45 GPa), the experimental data fall on the calculated compression curve corresponding to the (A-HS, B-HS) state. Starting from ~45 GPa, the data points deviate from the (A-HS, B-HS) curve and then join the (A-HS, B-LS) curve at ~60 GPa. Starting from ~100 GPa, the data deviate from the curve again. This, however, is very likely to result from the questionable accuracy of the Au pressure scale used in the experiment, as already discussed in the case of (Mg, Fe)SiO_3 Pv [44]. Notice that the observed volume reduction further confirms the B-site HS-LS crossover, as the previously perceived A-site HS-LS crossover barely leads to a volume reduction, evident from the compression curves (A HS, B LS and A LS, B LS) shown in Fig. 4(a). The B-site spin-state crossover and the observed volume reduction in the 45–60 GPa range can be qualitatively understood via the Fe^{3+} electronic configurations and Fe-O distances at A and B sites. With all $3d$ orbitals occupied, HS iron has spherically shaped electron charge density and the largest radius compared with other spin states, favoring longer Fe-O distances. Residing in the large dodecahedral cage, the A-site iron can easily maintain longer Fe-O distances and thus remain in HS state. In contrast, the Fe-O octahedron has smaller size and shorter Fe-O distances. With increasing pressure, the internal octahedron bond lengths can be shortened enough to induce the HS-LS crossover. Since the $3d$ electrons of the B-site LS iron *only* occupy the t_{2g}-like orbitals pointing away

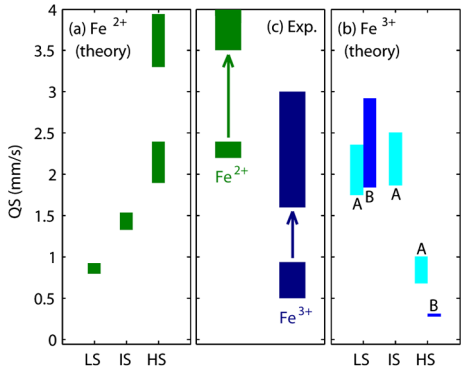

FIG. 3 (color online). Calculated QSs of (a) ferrous iron [27] and (b) ferric iron in $MgSiO_3$ Pv. Letters A and B in (b) refer to iron-occupying site. Arrows in (c) indicate the measured effect of pressure on QSs [16,18,30].

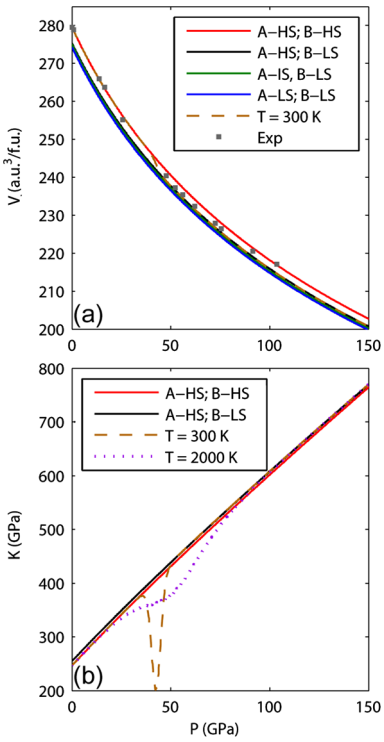

FIG. 4 (color online). Compression curves (a) and bulk modulus (b) of $(Mg_{1-x}Fe_x)(Si_{1-x}Fe_x)O_3$ Pv computed with LDA + U_{sc} ($x = 0.125$) and room-temperature measurements ($x = 0.1$) [30]. Both the measured and calculated compression curves exhibit a clear reduction accompanying the B-site HS-LS crossover, which leads to a softening in bulk modulus shown in (b).

from oxygen, the associated Fe-O distances are significantly shorter than those of the HS iron at the same pressure. Therefore, the spin change of the *B*-site iron is accompanied by a noticeable octahedral (and thus unit-cell) volume reduction. Such volume reduction leads to anomalous softening in bulk modulus, as described below.

At finite temperatures, the spin-state crossover passes through a mixed-spin (MS) state (namely, HS and LS coexist) within a finite pressure range that increases with temperature. During the crossover, the thermodynamic properties of the MS state exhibit anomalous behavior that may affect mantle properties. One example is the softening in bulk modules and its effect on the compressional wave velocity, as already seen in ferropericlase [7,10,11]. To estimate such anomaly in (Mg, Fe)(Si, Fe)O_3 Pv, we employ a thermodynamic model similar to that used in Ref. [10]. Here, we do not include vibrational free energy, as it barely affects the magnitude of the anomaly, slightly increases the transition pressure, and uniformly decreases the bulk modulus, as shown in the case of ferropericlase [10,11]. Indeed, the calculated $V(P)$ curve of (Mg, Fe)(Si, Fe)O_3 Pv in the MS state (using LDA + U_{sc}) at room temperature (300 K), shown as the dashed line in Fig. 4(a), exhibits a volume reduction ($\sim 1.2\%$) around the predicted P_T, 41 GPa. This reduction leads to a significant softening in bulk modulus, as shown in Fig. 4(b). The softening is still prominent at 2000 K, the temperature near the top of the lower mantle (~ 660 km deep). Given the abundance of iron-bearing Pv and the possibly high population of ferric iron, this softening may have a noticeable impact on the mantle properties, including possible anomalies in the seismic wave velocities.

In summary, with a series of DFT + U calculations, we have shown that the actual ground state of (Mg, Fe)(Si, Fe)O_3 perovskite has high-spin ferric iron on both *A* and *B* sites. It is the *B*-site ferric iron that undergoes a crossover from high-spin to low-spin state with increasing pressure, while the *A*-site iron remains in the high-spin state. The calculated quadrupole splittings and the compression curves are consistent with experiments. The volume reduction accompanying the *B*-site HS-LS crossover leads to a significant softening in bulk modulus, which suggests a possible source of seismic-velocity anomalies in the lower mantle. This work, one more time, demonstrates that the nuclear hyperfine interaction, combined with first-principles calculations, can be a useful tool to identify the spin states of transition-metal ions in solids under high pressures.

This work was primarily supported by the MRSEC Program of NSF under Grants No. DMR-0212302 and No. DMR-0819885, and partially supported by EAR-081272, EAR-1047629, and ATM-0426757 (VLab). P. B. was supported by the Austrian Science Fund (SFB F41, "ViCoM"). Calculations were performed at the Minnesota Supercomputing Institute (MSI).

[1] *Spin Crossover in Transition Metal Complexes I–III*, Topics in Current Chemistry Vols. 233–235, edited by P. Gütlich and H. A. Goodwin (Springer, New York, 2004).
[2] J. Badro *et al.*, Science **300**, 789 (2003).
[3] J.-F. Lin *et al.*, Nature (London) **436**, 377 (2005).
[4] I. Y. Kantor, L. S. Dubrovinsky, and C. A. McCammon, Phys. Rev. B **73**, 100101(R) (2006).
[5] J.-F. Lin *et al.*, Science **317**, 1740 (2007).
[6] T. Tsuchiya *et al.*, Phys. Rev. Lett. **96**, 198501 (2006).
[7] J. Crowhurst *et al.*, Science **319**, 451 (2008).
[8] A. F. Goncharov *et al.*, Science **312**, 1205 (2006).
[9] J.-F. Lin *et al.*, Geophys. Res. Lett. **34**, L16 305 (2007).
[10] R. M. Wentzcovitch *et al.*, Proc. Natl. Acad. Sci. U.S.A. **106**, 8447 (2009).
[11] Z. Wu *et al.*, Phys. Rev. B **80**, 014409 (2009).
[12] J.-F. Lin and T. Tsuchiya, Phys. Earth Planet. Inter. **170**, 248 (2008), and references therein.
[13] Han Hsu *et al.*, Rev. Mineral. Geochem. **71**, 169 (2010), and references therein.
[14] J. Badro *et al.*, Science **305**, 383 (2004).
[15] J. Li *et al.*, Proc. Natl. Acad. Sci. U.S.A. **101**, 14 027 (2004).
[16] J. M. Jackson *et al.*, Am. Mineral. **90**, 199 (2005).
[17] J. Li *et al.*, Phys. Chem. Miner. **33**, 575 (2006).
[18] C. McCammon *et al.*, Nat. Geosci. **1**, 684 (2008).
[19] J.-F. Lin *et al.*, Nat. Geosci. **1**, 688 (2008).
[20] A. M. Hofmeister, Earth Planet. Sci. Lett. **243**, 44 (2006).
[21] F. Zhang and A. R. Oganov, Earth Planet. Sci. Lett. **249**, 436 (2006).
[22] S. Stackhouse *et al.*, Earth Planet. Sci. Lett. **253**, 282 (2007).
[23] A. Bengtson, K. Persson, and D. Morgan, Earth Planet. Sci. Lett. **265**, 535 (2008).
[24] K. Umemoto *et al.*, Earth Planet. Sci. Lett. **276**, 198 (2008).
[25] K. Umemoto, H. Hsu, and R. M. Wentzcovitch, Phys. Earth Planet. Inter. **180**, 209 (2010).
[26] A. Bengtson *et al.*, Geophys. Res. Lett. **36**, L15 301 (2009).
[27] Han Hsu *et al.*, Earth Planet. Sci. Lett. **294**, 19 (2010).
[28] C. McCammon, Nature (London) **387**, 694 (1997).
[29] D. Frost *et al.*, Nature (London) **428**, 409 (2004).
[30] K. Catalli *et al.*, Earth Planet. Sci. Lett. **289**, 68 (2010).
[31] Han Hsu *et al.*, Phys. Rev. B **82**, 100406(R) (2010).
[32] R. M. Wentzcovitch, J. L. Martins, and G. D. Price, Phys. Rev. Lett. **70**, 3947 (1993).
[33] P. Giannozzi *et al.*, J. Phys. Condens. Matter **21**, 395502 (2009).
[34] The pseudopotentials used in this work are the same as those in Ref. [24].
[35] G. Madsen *et al.*, Phys. Rev. B **64**, 195134 (2001).
[36] P. Blaha *et al.*, WIEN2K, edited by K. Schwarz, Technische Universität Wien, Vienna, 2001.
[37] H. M. Petrilli *et al.*, Phys. Rev. B **57**, 14 690 (1998).
[38] M. Cococcioni and S. de Gironcoli, Phys. Rev. B **71**, 035105 (2005).
[39] H. Kulik *et al.*, Phys. Rev. Lett. **97**, 103001 (2006).
[40] V. L. Campo, Jr. and M. Cococcioni, J. Phys. Condens. Matter **22**, 055602 (2010).
[41] See supplemental material at http://link.aps.org/supplemental/10.1103/PhysRevLett.106.118501 for the calculation of self-consistent U and the electronic density of states of (Mg, Fe)(Si, Fe)O_3.
[42] M. Swart *et al.*, J. Phys. Chem. A **108**, 5479 (2004).
[43] A. Fouqueau *et al.*, J. Chem. Phys. **122**, 044110 (2005).
[44] Han Hsu *et al.*, Phys. Earth Planet. Inter. **185**, 13 (2011).